Asian Journal of Chemistry; Vol. 38, No. 9 (2026), 2363-2370
ASIAN JOURNAL OF CHEMISTRY
https://doi.org/10.14233/ajchem.2026.36339

Characterization of Netupitant Degradation Products Employing LC-QTOF-MS and Computational Tools

BHAVNA MAHAJAN[1,*], PANKAJ MINIYAR[2,3], RAHUL CHODANKAR[4], ANAND MAHAJAN[5] and MORESHWAR MAHAJAN[6]

[1]Department of Pharmaceutical Chemistry, Faculty of Pharmacy, Vishwakarma University, Pune-411048, India
[2]Department of Pharmaceutical Chemistry, Faculty of Pharmacy, D.Y. Patil University, Pune-410507, India
[3]Department of Pharmaceutical Chemistry, Faculty of Pharmacy, Savitribai Phule Pune University, Pune-411007, India
[4]Department of Pharmaceutical Chemistry, Faculty of Pharmacy, Goa College of Pharmacy, Panaji-403001, India
[5]Department of Pharmaceutical Analysis, Faculty of Pharmacy, Goa College of Pharmacy, Panaji-403001, India
[6]Department of Pharmaceutical Chemistry, Faculty of Pharmacy, STES Sinhgad Institute of Pharmacy (Affiliated to Savitribai Phule Pune University, Pune), Pune-411041, India

*Corresponding author: E-mail: bhavnamahajan15@gmail.com

Received: 29 April 2026 *Accepted*: 4 August 2026 *Published online*: 5 September 2026 AJC-22464

The present study evaluates the stability of netupitant under various environmental stress conditions and identifies the degradation products formed during the degradation process. In addition, the study predicts the pharmacokinetic and toxicological properties of these degradation products using advanced analytical and computational approaches. Isocratic liquid chromatography was used to separate stress samples, high-resolution quadrupole time-of-flight mass spectrometry was used to elucidate the structure of these samples. Computational platforms were used in making predictions of toxicity and molecular docking simulations were performed to assess the relative binding affinities of the parent drug and its degradants to the human neurokinin-1 receptor. Netupitant was susceptible to oxidative and hydrolytic stress, mainly through oxidative cleavage of the piperazine ring. Molecular docking showed that netupitant has the best neurokinin-1 receptor binding affinity (-12.1 kcal/mol) and structural loss in the degradants slightly alters the binding affinity towards the receptor (between -11.3 and -10.2 kcal/mol). Shifting the degradation products through software screens comprising the pkCSM webserver, ToxTree and OSIRIS property explorer yielded predictions for various pharmacokinetic and toxicity-related parameters. The computational predictions highlighted high intestinal absorption and hepatotoxicity across all compounds, with specific mutagenic structural alerts identified in one degradation product and a tumorigenic alert in another.

Keywords: Netupitant, Degradation product, Liquid chromatography, Mass spectrometry.

INTRODUCTION

Netupitant-palonosetron (Akynzeo®, Nykron®) is a recently developed combination therapy for the prevention of chemotherapy-induced nausea and vomiting (CINV) in patients receiving various chemotherapy regimens [1]. Netupitant is a selective neurokinin-1 (NK1) receptor antagonist that inhibits the substance P signaling pathway, a key mediator of emesis in the central nervous system [2]. Palonosetron, a 5-hydroxytryptamine-3 (5-HT3) receptor antagonist, complements the action of netupitant by blocking serotonin-mediated signaling, another important pathway involved in the development of CINV [3,4]. By simultaneously targeting the NK1 and 5-HT3 receptor pathways, this combination provides an effective approach to the prevention of CINV, which remains a common and distressing complication of chemotherapy and can adversely affect patients' quality of life and adherence to treatment [5]. Therefore, the availability of effective antiemetic therapies such as netupitant-palonosetron is essential for improving the tolerability of chemotherapy and supporting treatment compliance.

Several analytical methods have been developed to investigate the pharmacokinetics, metabolism and degradation behaviour of netupitant, particularly using HPLC and LC-MS/MS techniques. Xu *et al.* [6] developed and validated an LC-MS/MS method for the determination of netupitant in human

plasma, which has been subsequently applied in several clinical pharmacokinetic studies. Chira *et al.* [7] employed an electrochemical approach coupled with mass spectrometry to investigate the oxidative metabolism of netupitant, providing valuable insights into its possible metabolic pathways. From a pharmaceutical quality-control perspective, Panigrahy & Reddy [8] and Raveendranath *et al.* [9] reported limited reverse-phase HPLC (RP-HPLC) methods for the simultaneous estimation of netupitant and palonosetron. However, these studies primarily focused on the determination of the parent drugs, with comparatively limited information available on the systematic characterization of netupitant degradation products under stress conditions.

Although previous studies have reported degradation products of netupitant under forced conditions, they were largely limited to quantitative assessment, with little information on the structural identity and formation pathways of these impurities. The present study addresses this gap by systematically evaluating the oxidative degradation of netupitant under ICH-recommended stress conditions and characterizing the resulting degradation products using LC-QTOF-MS. Their potential mutagenic and systemic toxicity was further assessed using *in silico* approaches in accordance with the principles of ICH M7. Molecular docking with the human NK1 receptor was also performed to evaluate the effect of structural modifications on receptor-binding interactions. This integrated approach provides insight into the degradation behaviour and potential safety implications of netupitant degradation products and establishes a basis for their future isolation and experimental evaluation.

EXPERIMENTAL

Zydus Lifesciences Ltd. (Ahmedabad, India) provided the netupitant active pharmaceutical ingredient. Netupitant tablet preparation (brand name Nykron, batch no. BEZ1282) was purchased at a local pharmacy. Reagents such as sodium hydroxide, hydrochloric acid, formic acid, ammonium acetate, ammonia solution and hydrogen peroxide, were of analytical grade and were obtained at Advent Laboratories.

Chromatographic separation was performed using a ThermoFisher Scientific HPLC system equipped with Chromeleon 7.3.2 software and a Hypersil BDS C18 column (250 mm × 4.6 mm, 5 µm particle size). Mass spectral analysis was carried out using an Agilent 1200 Series HPLC coupled to an Agilent 6550 UHD Accurate-Mass Q-TOF mass spectrometer. Other equipment included a precision analytical balance (Wensar), constant-temperature water bath (Labman), calibrated photostability chamber (Thermo-lab Scientific), hot-air oven (Thermo Scientific) and ultrasonic bath (Labman).

Computational tools: Molecular docking studies were performed on an Intel Core i7 workstation with 32 GB RAM running Windows 10. AutoDock Vina [10] was used to generate docking poses, while Maestro Viewer [11], Avogadro [12], MarvinSketch [13] and AutoDock Tools [14] were used for molecular visualization, structure preparation and analysis. Pharmacokinetic and toxicity profiles were predicted using the pkCSM, ToxTree and OSIRIS Property Explorer platforms [15,16].

Forced degradation studies: Stress testing was performed in accordance with international guidelines [17] to evaluate the stability of netupitant under conditions relevant to its pharmaceutical lifecycle. The drug was subjected to hydrolytic (acidic and alkaline), oxidative, thermal and photolytic stress conditions. For chemical stress studies, blank, stressed and corresponding unstressed control samples were analyzed. For thermal and photolytic studies, paired stressed and control samples were prepared for comparison.

Hydrolytic degradation: Acidic and alkaline hydrolysis were performed using 2 M HCl and 2 M NaOH, respectively. Netupitant solution (1.0 mL, 3000 µg/mL) was reacted with 1.0 mL of the respective stressor in separate 10 mL volumetric flasks. The acidic mixture was heated at 80 ºC for 3 h, while the alkaline mixture was heated at 80 ºC for 20 min. Both samples were neutralized, diluted to 10 mL with the mobile phase diluent and subjected to HPLC analysis (300 µg/mL).

Oxidative degradation: A 1 mL aliquot of netupitant solution (3000 µg/mL) was reacted with 1 mL of 6% H_2O_2 for 24 h at ambient temperature. A corresponding blank omitting the drug was prepared simultaneously. Following the 24 h exposure, samples were diluted to 10 mL with diluent prior to analysis (300 µg/mL).

Thermal degradation: Solid-state thermal degradation was evaluated by exposing the drug in a sealed glass ampoule to dry heat (80 ºC) in a hot air oven for 10 h. A parallel control ampoule was maintained at ambient temperature. After exposing, the samples were weighed correctly and dissolved in 10.0 mL of diluent to obtain a final concentration of 300 µg/mL.

Photolytic degradation: Photolytic stress in liquid phase was caused by addition of netupitant solutions (300 µg/mL) to 1.2 million lux-hours of fluorescent light and 200 watt-h/m^2 of ultraviolet light in a calibrated photostability chamber [18]. An Amber volumetric flask wrapped in an aluminium foil kept a control sample.

HPLC method development and sample preparation: A 3000 µg/mL solution of netupitant (as a primary stock solution) was prepared in acetonitrile. A diluent of acetonitrile and 10 mM ammonium acetate buffer (pH 9.0, pH adjusted with ammonia 90:10 (v/v) was used to prepare the working solutions. Any stressed or blank samples were diluted to an end result of 300 µg/mL, a concentration that had been tested and confirmed in the literature [8,9] to provide the best peak height. Separations were done by chromatography through isocratic elution using the above 90:10 (v/v) mobile phase. Netupitant weakly basic pK_a (9.72) required a mobile phase pH of 9.0 to maintain the optimum elution and peak symmetry [6]. The flow rate was set at 1.0 mL/min, injection volume was set at 10 µL and ultraviolet was set to 250 nm. Lastly, a mixture of all the stressed samples was examined to demonstrate the resolution of the parent drug and all of the formed degradation products on the baseline.

Analytical method validation: The stability-indicating assay method developed was validated according to accepted parameters of validation [19].

Specificity and selectivity: Specificity of method was determined by determining the parent drug/degradant chro-

matographic separation of the degradants. The purity of the peak was determined by a diode array detector.

Linearity: Linear response was assessed over 5 concentration levels 100-600 μg/mL. Triplicate injections were done and the linearity was established by the analysis of the linear regression of the peak area *versus* concentration.

Precision: Intra-day and inter-day precision were evaluated with six samples of the nominal assay concentration (300 μg/mL) on the same day and on successive days. The precision was in terms of relative standard deviation (RSD).

Accuracy: Spiking of the standard drug into a degradation mixture at 80, 100 and 120% of the nominal concentration (300 μg/mL) was used to perform recovery studies. All analyses were performed in triplicate and the mean percentage recovery was calculated.

Robustness and detection and quantification limits: Robustness was evaluated by introducing deliberate small variations in wavelength and flow rate, with results expressed as %RSD based on triplicate measurements for each variation. LOD and LOQ were determined statistically from the analytical data in accordance with ICH guidelines.

High-resolution mass spectrometry: The structural elucidation was performed using an LC-Q-TOF-MS system equipped with an electrospray ionization (ESI) source operated in positive-ion mode. Full-scan MS spectra were initially acquired at low collision energy to identify the precursor ions, followed by targeted MS/MS fragmentation of netupitant and its degradation products at a collision energy of 40 V. The optimized source parameters were: capillary voltage, 3400 V; sheath gas temperature, 350 ºC; sheath gas flow rate, 11 L/min; drying gas flow rate, 11 L/min and nebulizer pressure, 35 psi. Nitrogen was used as the drying, sheath and collision gas.

Molecular docking protocol: The crystal structure of the human neurokinin-1 (NK1) receptor in complex with netupitant (PDB ID: 6HLP) was obtained from the Protein Data Bank [20]. The receptor was prepared using Maestro by removing water molecules and co-crystallized ligands, except the native netupitant ligand. The docking grid was centered on the native ligand at x = 4.97, y = -2.25 and z = 32.54 Å, with a box size of 20 × 20 × 20 Å. Polar hydrogens and Kollman charges were added using AutoDock Tools. The degradation products were drawn in MarvinSketch and converted into 3D structures, followed by geometry optimization using Avogadro with the MMFF94 force field [21]. Gasteiger charges were assigned to the ligands using AutoDock Tools. Molecular docking was performed using the AutoDock Vina command-line interface with an exhaustiveness of 16 and 10 binding modes. The docking protocol was validated by re-docking native netupitant, which yielded an RMSD of 1.557 Å.

RESULTS AND DISCUSSION

The degradation behaviour of netupitant under different stress conditions is summarized in Table-1. Netupitant underwent degradation under acidic, alkaline, oxidative, thermal and photolytic conditions, with degradation products detected under each stress condition. Three major degradation products, designated DP-I, DP-II and DP-III according to their elution order, were identified. The proposed degradation pathways are shown in Fig. 1. DP-I was consistently observed under acidic, alkaline, photolytic and thermal stress conditions, as supported by its consistent relative retention time. DP-II was observed only under acidic stress, whereas DP-III was formed specifically under H_2O_2 stress. The formation pattern of these products points to distinct degradation pathways, with DP-I representing a common degradation product under several stress conditions and DP-II and DP-III being associated with specific chemical environments (Fig. 2).

Method development and optimization: A selective stability-indicating assay method (SIAM) was developed and optimized to achieve adequate separation of netupitant from its degradation products. Initial chromatographic experiments involved variation of the organic modifier, using methanol or acetonitrile, together with adjustment of the aqueous-phase pH. Since netupitant contains basic functional groups, particularly the piperazine moiety, acidic mobile phases resulted in poor retention and pronounced peak tailing, which can be attributed to secondary interactions with residual silanol groups on the stationary phase. An alkaline mobile phase consisting of 10 mM ammonium acetate adjusted to pH 9.0 provided improved chromatographic behaviour. Under these conditions, reduced ionization of the basic drug enhanced retention and resulted in sharper, more symmetrical peaks. Acetonitrile was selected over methanol because its lower viscosity provided better chromatographic efficiency and peak resolution.

The optimized chromatographic conditions consisted of isocratic elution with acetonitrile and 10 mM ammonium acetate buffer (pH 9.0) in a 90:10 (v/v) ratio. A Hypersil BDS C18 column (250 mm × 4.6 mm, 5 μm) provided suitable hydrophobic interaction and effective separation of netupitant from its stress-related impurities. The flow rate was maintained at 1.0 mL/min and detection was performed at 250 nm. The method met the predefined system-suitability require-

TABLE-1
QUANTITATIVE DEGRADATION DATA OF NETUPITANT UNDER DIFFERENT STRESS CONDITIONS

Medium	Temp. (ºC)	Time	Degradation (%)	Retention time (min)
Untreated	25	–	–	7.433
2 N HCl	80	3 h	7.56	3.700 (DP-I)
			5.12	5.300 (DP-II)
2 N NaOH	80	20 min	5.05	3.700 (DP-I)
Neutral hydrolysis	80	24 h	Nil	–
6% H_2O_2	25	24 h	6.73	9.700 (DP-III)
Thermal	80	10 h	5.32	3.550 (DP-I)
'Fluorescent light 1.2 million lux h' and 'UV light 200 Whm^{-2}'	25	72 h	5.22	3.553 (DP-I)

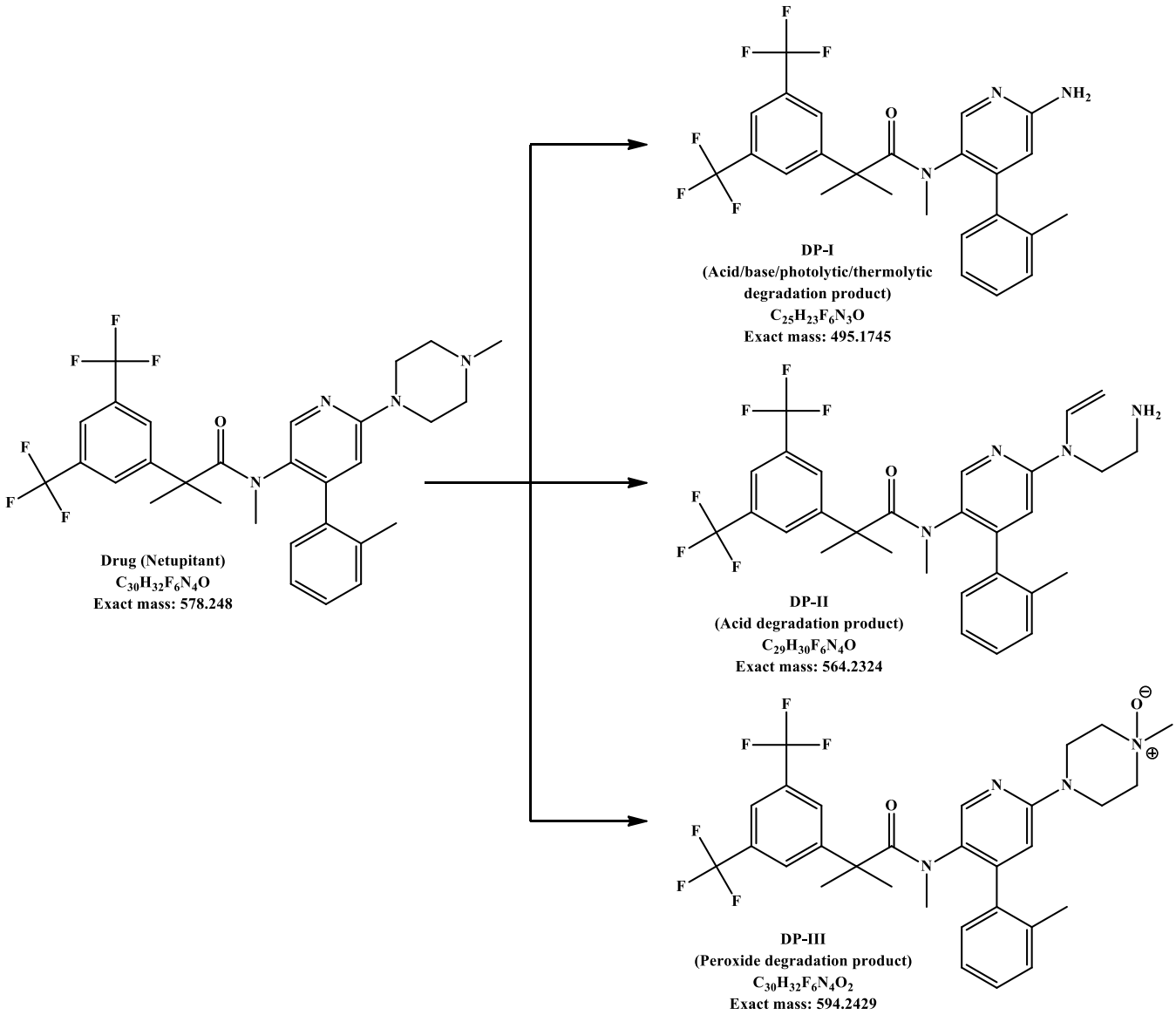

Fig. 1. Degradation pathway of netupitant

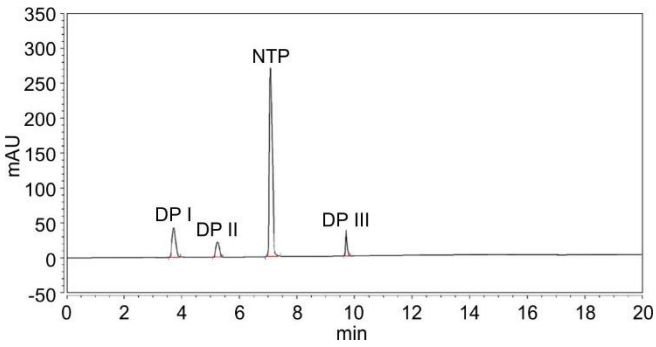

Fig. 2. Degradation product chromatogram of netupitant

ments, with a capacity factor (k) >1, resolution (R_s) >1.5, tailing factor (T_f) <1.5 and theoretical plate count (N) >2000 for the eluted components. Peak-purity assessment confirmed the spectral purity of the netupitant peak and the absence of co-eluting degradation impurities. Deliberate minor variations in flow rate, mobile-phase composition and pH did not adversely affect the chromatographic performance, supporting the robustness of the developed SIAM.

Specificity and selectivity: The developed method provided selective separation of netupitant and its degradation products. Netupitant, DP-I, DP-II and DP-III were resolved at baseline under the optimized chromatographic conditions. Blank samples subjected to the respective stress conditions did not exhibit interfering peaks at the retention times of the drug or degradation products. Diode-array detector peak-purity analysis gave purity values of ≥99% for the resolved peaks, supporting the absence of significant co-eluting components.

Linearity and range: The method exhibited a linear response over the concentration range of 100-600 µg/mL. A plot of peak area against concentration gave the regression equation $y = 17.089x - 16.267$, with a correlation coefficient (R^2) of 0.9996. The high correlation coefficient confirms the suitability of the method for quantitative determination of netupitant within the investigated concentration range.

Precision: Precision was evaluated using six independent preparations at the nominal assay concentration of 300 μg/mL on the same day and on consecutive days to assess intra-day and inter-day precision, respectively. The %RSD values were below 2% for both precision studies, satisfying conventional analytical acceptance criteria.

Accuracy: Accuracy was assessed through recovery studies by spiking known quantities of netupitant into a composite mixture of stressed samples at 80, 100 and 120% of the target assay concentration. The recovery values ranged from 99.0 to 101.0%, with an overall mean recovery of 100.4%.

Robustness, detection and quantification limits: The robustness of the method was assessed by deliberate changes in wavelength and flow rate, with triplicate analysis performed for each variation. The corresponding %RSD values were 0.36 and 0.65%, respectively, confirming that minor changes in these parameters did not substantially affect the analytical response. The LOD and LOQ were 3.21 and 9.74 μg/mL, respectively, as calculated statistically from the analytical data in accordance with ICH recommendations.

LC-Q-TOF-MS characterization of netupitant and degradation products: High-resolution LC-Q-TOF-MS analysis was performed to characterize netupitant and its three major degradation products and to establish their proposed structures and fragmentation pathways. The accurate-mass data are summarized in Table-2. The fragmentation behaviour of the parent drug provided a basis for interpreting the structural changes associated with each degradation product.

Fragmentation behaviour of netupitant: Netupitant exhibited a protonated molecular ion at *m/z* 579.2562. The collision-induced dissociation generated five principal product ions at *m/z* 522.1985, 255.0615, 241.0458, 227.0295 and 213.0123. The fragment at *m/z* 522.1985 can be attributed to cleavage involving the piperazine moiety, while further fragmentation generated the *m/z* 255.0615 ion through loss of the *N*-(6-(dimethylamino)-4-*o*-tolylpyridin-3-yl)-*N*-methylacetamide substructure. The ions at *m/z* 241.0458, 227.0295 and 213.0123 arise from successive neutral losses of alkyl groups associated with the 1,3-*bis*(trifluoromethyl)-5-isopropylbenzene moiety, with a regular mass difference of 14 Da. The fragmentation pattern is consistent with previously reported metabolic and bioanalytical data for netupitant by Xu *et al*. [6] and Chira *et al*. [7].

Characterization of DP-I: DP-I was detected as a major degradation product under several stress conditions and was assigned the structure 2-(3,5-*bis*(trifluoromethyl)phenyl)-*N*-(6-amino-4-*o*-tolylpyridin-3-yl)-*N*,2-dimethylpropanamide. Its molecular ion at *m/z* 496.1803 represents substantial modification of the piperazine-containing portion of netupitant, consistent with cleavage of the piperazine ring and formation of a primary aromatic amine. Ring-opening degradation of piperazine-containing pharmacophores has been reported for structurally related compounds [22-24]. MS/MS fragmentation of DP-I generated ions at *m/z* 255.0609, 241.0435, 227.0293 and 213.0143. The *m/z* 255.0609 ion corresponds to loss of the *N*-(6-amino-4-*o*-tolylpyridin-3-yl)-*N*-methylacetamide moiety, while the lower-mass ions follow the homologous fragmentation pattern observed for netupitant. The presence of the primary aromatic amine in DP-I is of particular interest from a toxicological perspective and was considered further in the *in silico* assessment.

Characterization of DP-II: DP-II exhibited a molecular ion at *m/z* 565.2048 and was assigned the proposed structure 2-(3,5-*bis*(trifluoromethyl)phenyl)-*N*-(6-(N-(2-aminoethyl)-*N*-vinylamino)-4-*o*-tolylpyridin-3-yl)-N,2-dimethylpropanamide. The observed mass shift relative to netupitant is consis-

TABLE-2
LC-QTOF-MS DATA FOR NETUPITANT AND ITS DEGRADATION PRODUCTS

Compound	m.f.	Theoretical mass (*m/z*)	Experimental mass (*m/z*)	Error (ppm)
Netupitant	$C_{30}H_{33}F_6N_4O^+$	579.2553	579.2565	2.1
Fragments	$C_{27}H_{26}F_6N_3O^+$	522.1974	522.1985	2.1
	$C_{11}H_9F_6^+$	255.0603	255.0615	4.6
	$C_{10}H_7F_6^+$	241.0446	241.0458	4.9
	$C_9H_5F_6^+$	227.029	227.0295	2.1
	$C_8H_3F_6^+$	213.0133	213.0123	-4.6
DP-I	$C_{25}H_{24}F_6N_3O^+$	496.1818	496.1803	-3.0
Fragments	$C_{11}H_9F_6^+$	255.0603	255.0609	2.3
	$C_{10}H_7F_6^+$	241.0446	241.0435	-4.7
	$C_9H_5F_6^+$	227.029	227.0293	1.2
	$C_8H_3F_6^+$	213.0133	213.0143	4.6
DP-II	$C_{28}H_{27}F_6N_4O_2^+$	565.2032	565.2048	2.9
Fragments	$C_{27}H_{26}F_6N_3O^+$	522.1974	522.1962	-2.3
	$C_{11}H_9F_6^+$	255.0603	255.0609	2.5
	$C_{10}H_7F_6^+$	241.0446	241.0456	4.3
	$C_9H_5F_6^+$	227.029	227.0294	1.8
	$C_8H_3F_6^+$	213.0133	213.0138	2.4
DP-III	$C_{30}H_{33}F_6N_4O_2^+$	595.2502	595.2517	2.6
Fragments	$C_{26}H_{24}F_6N_3O^+$	508.1818	508.1806	-2.3
	$C_{11}H_9F_6^+$	255.0603	255.0607	1.6
	$C_{10}H_7F_6^+$	241.0446	241.0453	2.9
	$C_9H_5F_6^+$	227.029	227.0281	-3.8
	$C_8H_3F_6^+$	213.0133	213.0138	2.4

tent with oxidative N-demethylation accompanied by modification and opening of the piperazine ring, in agreement with degradation behaviour reported for related piperazine containing structures [22-24]. The MS/MS spectrum contained product ions at *m/z* 255.0609, 241.0456, 227.0294 and 213.0138. Retention of these characteristic lower-mass fragments indicates preservation of the principal netupitant backbone after alteration of the piperazine substituent. The formation of DP-II specifically under acidic stress suggests that the modified piperazine structure has a distinct susceptibility to acid-mediated degradation.

Characterization of DP-III: Exposure to H_2O_2 resulted in formation of DP-III, assigned as 4-(5-(2-(3,5-*bis*(trifluoromethyl)phenyl)-*N*,2-dimethylpropanamido)-4-(*o*-tolyl)pyridin-2-yl)-1-methylpiperazine 1-oxide. Its protonated precursor ion appeared at *m/z* 595.2510, corresponding to an accurate mass increase of approximately 16 Da relative to netupitant and supporting the formation of an *N*-oxide at the piperazine nitrogen [22,24]. The susceptibility of the piperazine nitrogen to oxidation is consistent with stability concerns reported for netupitant in the European Medicines Agency assessment [25]. MS/MS fragmentation of DP-III generated a major product ion at *m/z* 508.1806, attributable to the oxidized piperazine moiety, together with secondary ions at *m/z* 255.0607, 241.0456, 227.0281 and 213.0138. The latter ions retain the characteristic fragmentation signature of the parent compound, confirmed the proposed N-oxide structure.

Proposed degradation pathways and differential chemical stability: The LC-Q-TOF-MS findings provide a basis for interpreting the distinct degradation behaviour of netupitant under hydrolytic and oxidative conditions. Despite exposure to acidic and alkaline stress, no prominent amide-hydrolysis products corresponding to the carboxylic acid or free amine fragments were detected. This behaviour suggests considerable resistance of the central tertiary amide bond toward hydrolysis. Steric protection around the amide functionality may contribute to this stability. The amide nitrogen is N-methylated and is associated with the bulky 2-[3,5-bis(trifluoromethyl)-phenyl]-2-methylpropanoyl group, forming substantial steric congestion around the amide linkage. A comparable steric effect has been described for the 2,6-dimethylphenyl moiety of lidocaine [26], where steric hindrance limits access of water or hydroxide ions to the amide bond and reduces the likelihood of the transition state required for hydrolysis.

The oxidative degradation pathway appears to be associated primarily with the electron-rich tertiary nitrogen of the piperazine ring. Oxidative stress may initiate single-electron transfer from this nitrogen to the oxidizing species, generating a transient nitrogen-centered radical cation. Hydrogen atom abstraction at the adjacent α-methylene position can then generate a resonance-stabilized α-aminoalkyl carbon radical. Reaction of this intermediate with molecular oxygen or peroxide species can form a reactive peroxyl radical (R–OO$^{\bullet}$), whose subsequent decomposition may give rise to an electrophilic iminium intermediate. Nucleophilic attack by water on such an intermediate provides a plausible route for C–N bond cleavage and piperazine-ring opening. Direct oxygen transfer to the piperazine nitrogen may provide an alternative pathway through *N*-oxide formation, followed by rearrangement or Polonovski-type fragmentation. Such pathways are chemically consistent with the formation of 2º amines, aminoethyl derivatives, aldehydic products and the *N*-oxide structure proposed for DP-III [27].

Molecular docking analysis: Molecular docking simulations were performed against the human NK1 receptor to assess whether structural changes associated with degradation could alter the receptor-binding behaviour of netupitant. The docking results are shown in Figs. 3 and 4. Netupitant exhibited the strongest predicted binding affinity, with a docking score of -12.1 kcal/mol. Its interaction with the receptor was largely supported by hydrophobic contacts within the active-site environment. Modification of the piperazine moiety was associated with progressively weaker predicted binding.

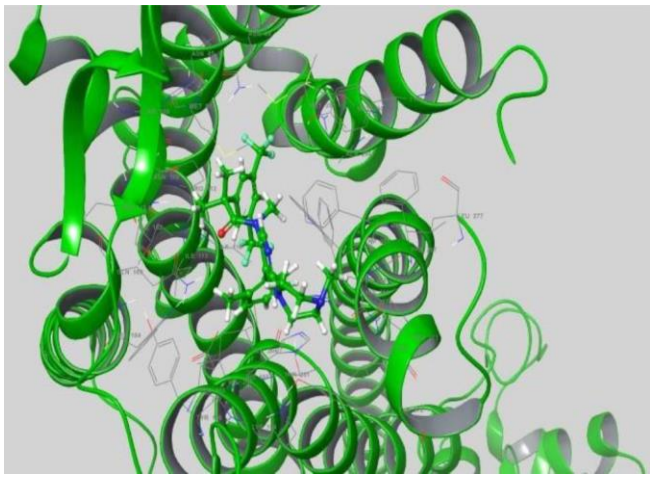

Fig. 3. Netupitant in the binding pocket of neurokinin receptor (PDB id: 6HLP)

DP-III, which retains the piperazine framework but carries an N-oxide group, gave a docking score of -11.3 kcal/mol. The localized charge associated with the N-oxide may alter the hydrophobic environment required for optimal receptor interaction. DP-I, which undergoes extensive structural modification of the piperazine region, exhibited a docking score of -11.0 kcal/mol. DP-II, with the most extensive modification of the piperazine-derived portion, gave the weakest predicted affinity at -10.2 kcal/mol. The docking results suggest that oxidative modification and structural disruption of the piperazine moiety can alter the predicted interaction of netupitant-derived species with the NK1 receptor, although these computational findings require experimental pharmacological confirmation.

***In silico* ADMET and toxicological assessment:** The predicted ADMET profiles of netupitant and its degradation products were evaluated using the pkCSM platform. Netupitant and all three proposed degradants were predicted to have high intestinal absorption, with values above 90% and each compound was predicted to act as a P-glycoprotein (P-gp) substrate. The calculated log BB values were below 0.3, corresponding to limited predicted penetration across the blood–brain barrier. The compounds were not predicted to inhibit CYP1A2 or CYP2D6. DP-I was predicted to inhibit CYP2C19, while DP-III was predicted to inhibit CYP2C9. Netupitant and DP-I were predicted to have potential CYP3A4 inhibitory activity.

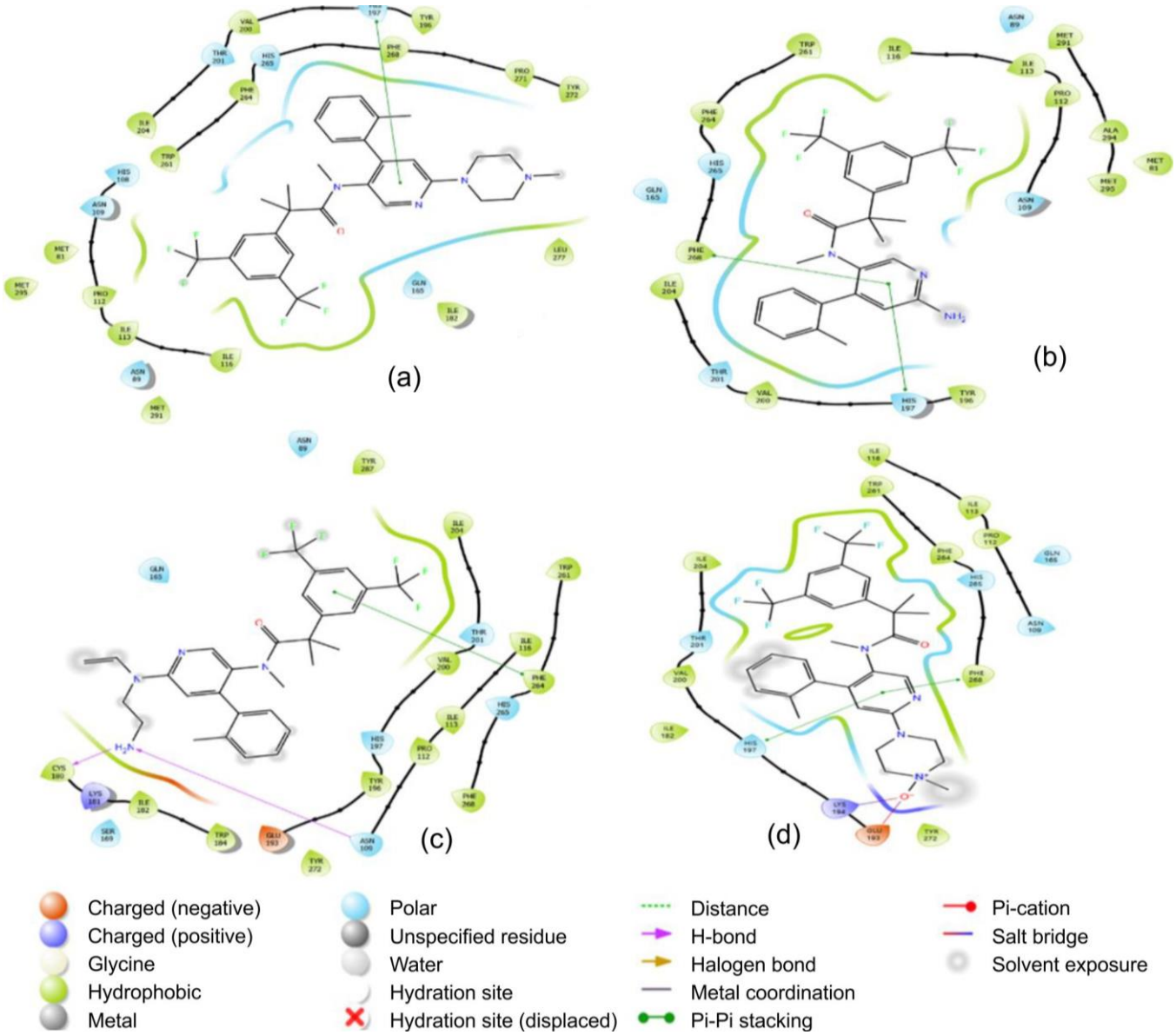

Fig. 4. Binding interactions (a) Netupitant, (b) DP-I, (c) DP-II and (d) DP-III

The toxicological screening provided further insight into structural changes associated with degradation. pkCSM predicted hepatotoxicity for the parent compound and the investigated degradation products, while no mutagenic liability was predicted by this platform. A complementary structural-alert assessment using *S. toxicarum* ToxTree identified a significant mutagenic structural alert for DP-I. This alert may be associated with the primary aromatic amine generated following piperazine-ring cleavage, a structural feature recognized as a potential toxicophore due to its possible involvement in DNA-reactive processes. OSIRIS Property Explorer did not predict tumorigenic potential for netupitant, DP-I or DP-III, whereas DP-II returned a positive tumorigenicity prediction. The investigated compounds were generally predicted to have no significant irritant or reproductive-toxicity liabilities.

The combined analytical and computational findings establish a relationship between the chemical instability of the piperazine moiety, the structures of the resulting degradation products, their predicted receptor interactions and their potential toxicological liabilities. The LC-Q-TOF-MS data support distinct structural pathways for DP-I, DP-II and DP-III, while the docking and toxicity predictions provide an initial assessment of the possible pharmacological and safety consequences of these structural changes. Since these findings are based partly on computational predictions, experimental isolation, structural confirmation, receptor-binding studies and toxicological evaluation of the individual degradation products would be required for definitive assessment.

Conclusion

A comprehensive forced-degradation study of netupitant was performed in accordance with ICH Q1A(R2) to establish the intrinsic stability profile of netupitant. The drug exhibited marked resistance to amide hydrolysis under acidic and alkaline conditions, which may be attributed to steric protection around its central tertiary amide group. The piperazine moiety

was identified as the principal site of chemical degradation under the investigated stress conditions. High-resolution LC-QTOF-MS enabled the characterization of three major degradation products with distinct fragmentation patterns. DP-I was detected under several stress conditions and was associated with the piperazine-ring cleavage, DP-II was observed under acidic stress, while DP-III was formed selectively under peroxide stress through *N*-oxidation. *In silico* ADMET and toxicological assessment using pkCSM, ToxTree and OSIRIS identified potential safety concerns among the degradation products. The primary aromatic amine presents in DP-I was associated with a predicted mutagenic structural alert, while the computational models also indicated potential hepatotoxicity and other metabolic accountabilities. Molecular docking against the human NK1 receptor revealed a progressive reduction in predicted binding affinity following structural modification of the piperazine moiety, with the parent drug exhibiting the strongest predicted interaction. These findings established a link between the chemical degradation of netupitant, structural changes in its degradation products and their predicted pharmacological and toxicological profiles.

CONFLICT OF INTEREST

The authors declare that there is no conflict of interests regarding the publication of this article.

DECLARATION OF AI-ASSISTED TECHNOLOGIES

During the preparation of this manuscript, the authors used an AI-assisted tool(s) to improve the language and no data, results or scientific conclusions were generated by AI. All analyses, interpretations and conclusions are the authors' own. The authors reviewed and edited the content and take full responsibility for the published work.

REFERENCES

1. C.A. Thompson, *Am. J. Health-Syst. Pharm*., **71**, 2000 (2014); https://doi.org/10.2146/news140079
2. C. Rojas, M. Stathis, A.G. Thomas, E.B. Massuda, J. Alt, J. Zhang, E.B. Rubenstein, S. Sebastiani, S. Cantoreggi, S.H. Snyder and B. Slusher, *Anesth. Analg*., **107**, 469 (2008); https://doi.org/10.1213/ane.0b013e318172fa74
3. C. Rojas, A.G. Thomas, J. Alt, M. Stathis, J. Zhang, E.B. Rubenstein, S. Sebastiani, S. Cantoreggi and B.S. Slusher, *Eur. J. Pharmacol*., **626**, 193 (2010); https://doi.org/10.1016/j.ejphar.2009.10.002
4. C. Rojas, Y. Li, J. Zhang, M. Stathis, A.G. Thomas, S. Cantoreggi, J. Alt, S. Sebastiani, C. Pietra and B.S. Slusher, *J. Pharmacol. Exp. Ther*., **335**, 362 (2010); https://doi.org/10.1124/jpet.110.166181
5. C.C. Sun, D.C. Bodurka, C.B. Weaver, R. Rasu, J.K. Wolf, M.W. Bevers, J.A. Smith, J.T. Wharton and E.B. Rubenstein, *Support. Care Cancer*, **13**, 219 (2005); https://doi.org/10.1007/s00520-004-0710-6
6. M. Xu, Y. Ni, S. Li, J. Du, H. Li, Y. Zhou, W. Li and H. Chen, *J. Chromatogr. B*, **1027**, 187 (2016); https://doi.org/10.1016/j.jchromb.2016.05.051
7. R. Chira, J. Fangmeyer, I.O. Neaga, V. Zaharia, U. Karst, E. Bodoki and R. Oprean, *J. Pharm. Anal*., **11**, 661 (2021); https://doi.org/10.1016/j.jpha.2021.03.011
8. U.P. Panigrahy and A.S.K. Reddy, *Int. J. ChemTech Res*., **8**, 317 (2015).
9. T.V. Raveendranath, R.T. Saravanakumar and C.H.K.V.L.S.N. Anjana, *Int. J. Pharm. Sci. Res*., **12**, 3693 (2021); https://doi.org/10.13040/IJPSR.0975-8232.12(7).3693-00
10. O. Trott and A.J. Olson, *J. Comput. Chem*., **31**, 455 (2010); https://doi.org/10.1002/jcc.21334
11. Schrödinger LLC, Schrödinger Release 2024-4: Maestro, New York (2024).
12. M.D. Hanwell, D.E. Curtis, D.C. Lonie, T. Vandermeersch, E. Zurek and G.R. Hutchison, *J. Cheminform*., **4**, 17 (2012); https://doi.org/10.1186/1758-2946-4-17
13. ChemAxon, Marvin 19.9.0, Budapest (2019).
14. G.M. Morris, R. Huey, W. Lindstrom, M.F. Sanner, R.K. Belew, D.S. Goodsell and A.J. Olson, *J. Comput. Chem*., **30**, 2785 (2009); https://doi.org/10.1002/jcc.21256
15. B.S. Mahajan, P.B. Miniyar, R.S. Chodankar and A.A. Mahajan, *Sep. Sci. Plus*, **7**, e202300223 (2024); https://doi.org/10.1002/sscp.202300223
16. B. Mahajan, P. Gawarkar-Patil, P. Adnaik, N. Bagade, P. Gondhale-Karpe, S. Manwatkar and S. Patil, in Biosystems, Biomedical & Drug Delivery Systems, Springer, Singapore pp. 311-326 (2024); https://doi.org/10.1007/978-981-97-2596-0_14
17. International Conference on Harmonisation, Stability Testing of New Drug Substances and Products Q1A(R2), Geneva (2003).
18. International Conference on Harmonisation, Photostability Testing of New Drug Substances and Products Q1B, Geneva (1996).
19. International Conference on Harmonisation, Validation of Analytical Procedures Q2(R1), Geneva (2005).
20. J. Schöppe, J. Ehrenmann, C. Klenk, P. Rucktooa, M. Schütz, A.S. Doré and A. Plückthun, *Nat. Commun*., **10**, 17 (2019); https://doi.org/10.1038/s41467-018-07939-8
21. B. S. Mahajan, L. A. Kawale, V. S. Nade, S. Unavane, L. Sajimon and P. Kapadnis, *Future J. Pharm. Sci*., **10**, 50 (2024); https://doi.org/10.1186/s43094-024-00626-0
22. M.V.V.N. Murali Krishna, S.V. Rao and N.V.S. Venugopal, *J. Liq. Chromatogr. Relat. Technol*., **40**, 741 (2017); https://doi.org/10.1080/10826076.2017.1357572
23. R.A. Osawa, B.T. Barrocas, O.C. Monteiro, M.C. Oliveira and M.H. Florêncio, *Chem. Eng. J*., **373**, 1338 (2019); https://doi.org/10.1016/j.cej.2019.05.137
24. M. Thummar, P.N. Patel, B.S. Kushwah and G. Samanthula, *New J. Chem*., **42**, 16972 (2018); https://doi.org/10.1039/C8NJ03545H
25. European Medicines Agency, Assessment Report: Akynzeo, Amsterdam (2015).
26. Y. Kadioglu, A. Atila, M.S. Gultekin and N.A. Alp, *Iran. J. Pharm. Res*., **12**, 659 (2013).
27. T. Wang and K.-J. Jens, *Int. J. Greenh. Gas Control*, **24**, 98 (2014); https://doi.org/10.1016/j.ijggc.2014.03.003